F 5 Physics of the malaria parasite

Ulrich S. Schwarz
Institute for Theoretical Physics and
BioQuant-Center for Quantitative Biology
Heidelberg University

Contents

Lecture Notes of the 49^{th} IFF Spring School "Physics of Life" (Forschungszentrum Jülich, 2018). All rights reserved.

1 Introduction

Malaria is one of the most devastating diseases that plague mankind [1]. It is caused by a unicellular eukaryotic parasite from the genus *Plasmodium* that is transmitted to humans through the bite of a female *Anopheles* mosquito. Although the malaria incidence rates have gone down significantly over the last years due to improved prevention measures (like use of mosquito nets), according to the latest estimate, in 2015 there were still 212 million cases and 429.000 deaths [2]. Since 2001, a total of 6.8 million malaria deaths have been estimated, with the main victims being under 5 years old children in Africa. Despite many efforts in this direction, there is still no vaccine available against malaria. The malaria parasite is extremely well adapted to its host organisms and its permanent struggle with the human host has strongly shaped our genome. In particular, there are several genetic diseases that in fact are favored by the presence of the malaria parasite, including mutations in the hemoglobin genes (such as the one leading to sickle cell amenia) and hereditary ovalo-, ellipto- and spherocytoses [3, 4].

Although research on malaria is still largely motivated by the search for new therapies and strongly focused on epidemiology, immunology and genetics, during the last decade there has been a growing effort to also address biophysical questions arising in the context of this disease [5, 6, 7, 8]. The relevance of biophysics becomes obvious if one considers the lifecycle of the malaria parasite in the human host, as shown in Fig. 1. It starts with an *Anopheles* mosquitos injecting several malaria sporozoites into the skin of the host during a blood meal. These then search for blood vessels and use the blood flow to travel to the liver, where one sporozoite can multiply into thousands of merozoites, that then are released into the blood, where they invade red blood cells (RBCs) (top right inset). The infected red blood cells (iRBCs) gets remodeled by the parasite and starts to become adhesive, e.g. to placenta and vascular endothelium (middle and bottom right insets, respectively). This increases the residency time in the vasculature and avoids clearance by the spleen, where RBCs that do not manage to squeeze through the 2 μm narrow interendothelial slits are sorted out by macrophages from the immune system [9, 10]. After 48 h, the iRBC ruptures and around 20 new merozoites are released, thus closing the asexual cycle. A small portion of the parasites become gametocytes. If taken up by a female mosquito, the parasites go through several mosquito stages, until they are injected again into a human host, so that the full infectious cycle is closed. Including all human and mosquito stages, the complete malaria cycle takes several weeks.

The first obvious questions to address with concepts and method from physics are how the malaria parasite manages to physically move through so many different parts of the human body (mainly skin, liver and blood) and how it invades and remodels compartments in the host (in particular RBCs). Because the medical symptoms of the disease (like fever and anemia) are mainly related to the blood stage, the second set of interesting biophysical questions centers around the way the malaria parasite changes the hydrodynamic movement of RBCs and their interactions with other cells in the vasculature (other RBCs, white blood cells, platelets and vascular endothelial cells). Most of these biophysics questions concern cell mechanics, cell adhesion and motion in hydrodynamic flow, which are well-developed subfields of cellular biophysics. Interestingly, similar biophysics questions as addressed here for the malaria parasite are increasingly asked also for other parasites, including *Toxoplasma*, *Leishmania* or *Trypanosoma* (the causative agents of sleeping sickness) [11, 12].

Here we will review recent progress regarding the biophysics of the malaria parasite. We start with an introduction to the malaria lifecycle and then discuss the most important feature of the skin stage, namely the surprisingly rapid movement through the skin of the host based

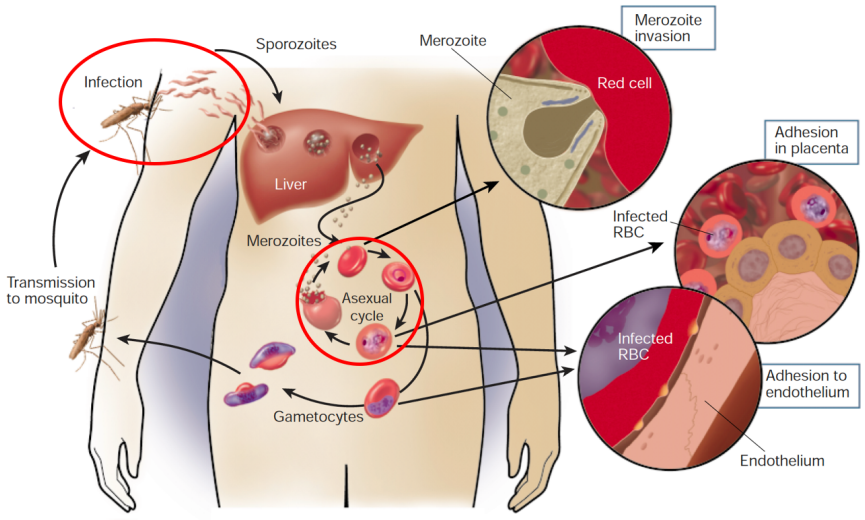

Fig. 1: *Lifecycle of the malaria parasite in the human body. The malaria parasite is injected into the skin in the form of sporozoites and first replicates in the liver. It then invades red blood cells (RBCs) in the form of merozoites. By replicating within RBCs and then rupturing them, it forms an asexual 48 h cycle in the blood. Some of the parasites become gametocytes and are taken up by another mosquito. In this review we discuss the skin and blood stages in more detail, which are here marked by red circles. Adapted from [1].*

with a special mode of locomotion called *gliding motility*. Interestingly, the same machinery underlying gliding motility is also used to invade RBCs. We will then discuss how the parasite remodels the iRBC and its interactions with the environment. In particular, we will discuss why and how it makes the iRBC adhesive (*cytoadherence*) and which consequences this will have for the movement of iRBCs in the vasculature. We finally conclude with a summary of some open questions.

2 The malaria lifecycle

2.1 Skin stage

Several species from the genus *Plasmodium* can transmit malaria, but the most fatal and therefore medically most important one is *Plasmodium falciparum*. A large range of imaging modalities, including confocal, intravital, two-photon, super-resolution, light sheet, electron and atomic force microscopies, have been employed to reveal the details of how the parasite moves and develops over the different stages of the lifecycle [13]. As shown in Fig. 1, the lifecycle starts when during the blood meal of a female mosquito tens of malaria parasites are injected into the skin of the host in the form of crescent-shaped *sporozoites*. A convenient model system to study sporozoite migration is the rodent parasite *Plasmodium berghei*, which does not infect humans. Fig. 2A shows the architecture of a mature sporozoite. Typical values for length, width and radius of curvature are 10 μm, 1 μm and 5 μm, respectively. At the right, one sees the apical polar ring (APR), that defines the front of the cell and through which it secretes various components required for motility and invasion. The shape of the sporozoite is fixed by the inner membrane complex (IMC), a system of flattened vesicles underlying the membrane, and the

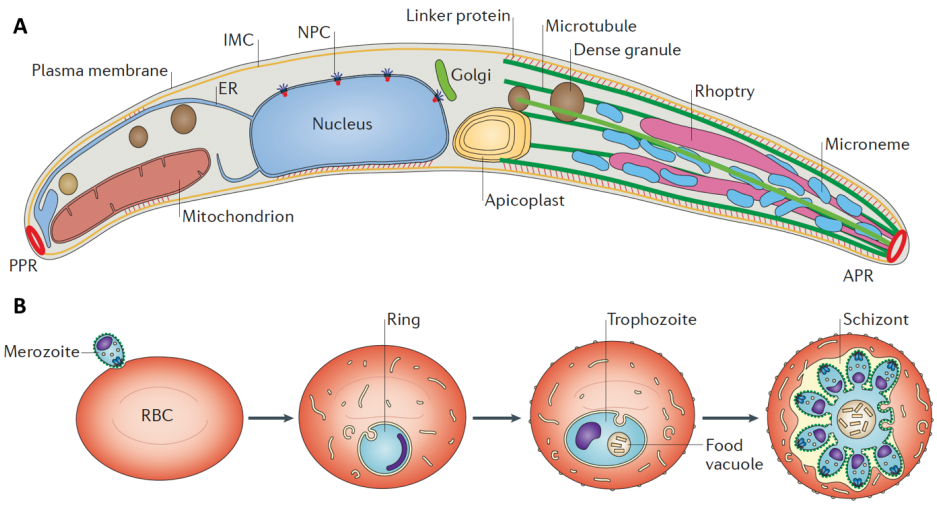

Fig. 2: *(A) Organization of a sporozoite, the crescent-shaped and highly motile form of the parasite during the skin stage. The cartoon clearly shows the polar structure of the cell, with an apical polar ring (APR) at the front and a posterior polar ring (PPR) at the back. (B) Organization of the iRBC over the 48 h asexual cycle of the blood stage. As the parasite mass grows, it moves into the center. The digested hemoglobin is collected in a food vacuole. Cartoons taken from [13].*

basket of microtubules anchored to the APR. The nucleus is located two thirds towards the back of the cell, which is defined by the posterior polar ring (PPR). Invasion and motility is closely related to myosin molecular motors, which together with a system of short actin filaments are located between the IMC and the plasma membrane. Together they effect a continuous flow of adhesion molecules from the APR to the PPR. Once these adhesion molecules engage with ligands in their environment, the cell itself is pushed forward.

Although earlier it had been believed that the sporozoites are directly injected into blood capillaries, today we know that usually they are deposited into the skin [14]. They then move rapidly through the connective tissue, with a typical speed of 1-2 μm/s and in locally helical trajectories, that arise from their crescent shape [15]. The crescent shape seems to be beneficial for circling around capillaries and finally invading them [16, 17]. In order to appreciate the high speed of these cells, one has to note that the typical speed for keratocyte and fibroblasts, which are the standard model systems for fast and normally migrating animal cells, are 0.2 μm/s [18] and less than 1 μm/min [19], respectively. Thus the malaria sporozoite holds the world record for a migrating cell (which however is still much lower than the typical speed range of 10-100 μm/s for microswimmers such as sperm or flagellated bacteria).

2.2 Liver stage

Once inside a blood capillary, blood flow passively carries the sporozoites towards the liver. There seem to be multiple entry pathways into the liver, including the Kupffer cells from the immune system that connect blood flow and liver. In the liver, malaria parasites multiply inside hepatocytes. One sporozoite is sufficient to have thousands of merozoites being released into the blood stream after 7-10 days, where they start to invade RBCs. At this stage, there are no

clinical symptoms yet of the infection.

2.3 Blood stage

The merozoite in the blood stage is the smallest cell of the lifecyle, with a typical size of 1-2 μm and an egg shape. The time before RBC-invasion is the only part of the lifecycle in which it is directly exposed to the host immune system, and it lasts only for a few minutes, because then merozoites quickly loose the ability to invade RBCs. Merozoite-invasion of RBCs is an intriguing process and has been studied in great detail as it might provide a way to stop propagation of the disease [20, 21, 22].
The first cartoon in Fig. 2B shows this very first part of the blood stage. After attachement, the merozoite quickly reorients with its apex towards the host membrane, with deformations waves emanating from the contact site [23]. A tight junction forms that during invasion moves over the merozoite within tens of seconds, driven by the same myosin molecular motor that also underlies sporozoite motility. Recently it has been suggested on theoretical grounds that the motor contribution can be relatively small as adhesive interactions with the membrane can account for large parts of the parasite re-orientation and wrapping [24]. Using optical tweezers to control contact between parasite and RBC, it has been shown that the adhesive forces are sufficiently strong to balance 40 pN forces [25]. Once the tight junction has reached the base of the cell, the membrane seals behind the parasite and forms the parasitophorous vacuole that the parasite now uses for its further development. Resealing is followed by another period of dramatic shape changes, during which the RBC forms multiple and evenly spaced projections on its surface (*echinocytosis*). It then returns to its normal biconcave shape within 10 minutes and the parasite starts to develop inside the iRBC.
During the 48 h until the iRBC is ruptured, the parasites produces and exports many proteins through the parasitophorous vacuole membrane (PVM), which together completely remodel the RBC. To feed its own metabolism, but also to convert the interior of the RBC into a normal cytoplasm, the parasite starts to digest hemoglobin . Because this increases osmotic pressure, at the same time the parasite establishes new permeation pathways in the host membrane, to control the osmotic pressure of the iRBC as described by the colloid-osmotic model [26]. It also starts to establish a systems of adhesive knobs on the surface of the iRBCs, by exporting structural proteins like the *knob-associated histidine-rich protein* (KAHRP) [27, 28, 29, 30], that self-assemble into spiral-shaped platforms below the membrane, and the adhesion protein *P. falciparum erythrocyte membrane protein 1* (PfEMP1), that inserts into these and can bind to a large range of extracellular adhesion molecules, including CSA, CD36 and ICAM1 [31, 32].
The spectrin network of the RBC is also completely remodeled: it becomes sparser away from the knobs and denser around the knobs [33, 34]. The junctional complexes in the spectrin network are dissolved and the actin of the protofilaments is used by the parasite to build actin filaments between the cell surface and newly induced membrane structures (*Maurer's clefts*) in the cytoplasm. Recently it has been argued that these actin filaments are essential transport pathways for the parasite, and that the sickle cell disease protects its carriers from malaria by impairing the build-up of these filaments [35, 4]. Effectively this then leads to reduced cytoadherence and increased clearance by the spleen, as observed earlier [32, 36].
The 48 h development inside the iRBC can be divided into ring (0-24 h), trophozoite (24-36 h) and schizont (40-48 h) stages, as shown in Fig. 2B [37, 13]. During the ring stage, the parasite stays close to the site of invasion, at the rim of the iRBC. At late ring stage, the first knobs start to appear on the iRBC-surface and the iRBC starts to adhere to the blood vessel walls. During

the trophozoite stage, the parasite mass becomes more rounded, moves to the center of the RBC and the end products of the hemoglobin digestion are collected in a growing food vacuole inside the parasite (*hemozoin*). Knob density increases to a value of around 10-30/μm^2 (depending on strain) and their typical diameter is 160 nm. Average spectrin length grows from 42 nm in wildtype to 64 nm in trophozoite [33].
During the schizont stage, the nucleus starts to divide asynchronously in a common syncytium, forming a flower structure with around 20 budding merozoites. Knob density further increases to a value of around 40-60/μm^2, while the diameter goes down to around 100 nm. The average spectrin length increases to 75 nm [33]. The Maurer's clefts initially move freely in the cytoplasm, but later are anchored to the cell surface.
Eventually the schizont rounds up and ruptures to release the new merozoites. Rupture is synchronized across iRBCs and leads to periodic fever in the patient. It has been shown that first the PVM and then the RBC-membrane opens, and that egress has a dispersive character, with merozoites being ejected in less than a second up to 10 μm into the environment [38]. Surprisingly, during merozoite ejection the host membrane curls away from the opening, indicating that the iRBC has built up some spontaneous curvature towards the outside [39]. Membrane curling is an obvious solution to quickly remove the membrane such that the merozoites have a high chance to encounter and invade nearby RBCs, thus closing the asexual cycle.

2.4 Other stages

The sexual part of the blood stage is not completely understood. Some parasites develop into *gametocytes* that seem to mature in RBCs in the bone marrow, in order to avoid clearance by the spleen. Mature gametocytes have to come back into the vasculature and then seem to be softer [40, 41]. Therefore they might be able to stay longer in the vasculature, until they are taken up during the blood meal of a female mosquito.
Once in the mosquito, female and male gametocytes fuse into *ookinetes*. These transverse the lumen of the mosquito midgut and develop into large *oocysts* on the outside of the mosquito gut. Until the oocysts rupture after approximately one week, hundreds of sporozoites are produced by asexual replication. In oocytes, the sporozoites are not able yet to move individually, but they do so collectively [42]. The sporozoites then move with the hemolymph to the salivary glands, where they acquire the individual ability for gliding motility. Although also very interesting from the biophysics point of view, the mosquito stages are not very well investigated, presumably because their medical relevance is not as large as the one of the stages in the vertebrate hosts.

3 Gliding motility of sporozoites

Like *Toxoplasma*, *Plasmodium* belongs to the genus of *Apicomplexa*, which move over external surfaces in a peculiar mode of locomotion called *gliding motility* [43, 44, 45, 22]. Gliding motility of *Plasmodium* and *Toxoplasma* also share some similarities with the adventurous motility of the bacterium *Myxococcus xanthus*, but there are also essential differences (in particular the chiral nature of the myxococcus gliding machinery) [46, 47, 48].
As shown in Fig. 2A, the sporozoite is a strongly polarized cells. Its apical ring at the front is used to secret various factors, which then are driven backwards over the surface of the cell by retrograde flow. Recently this retrograde flow has been measured by optical tweezer exper-

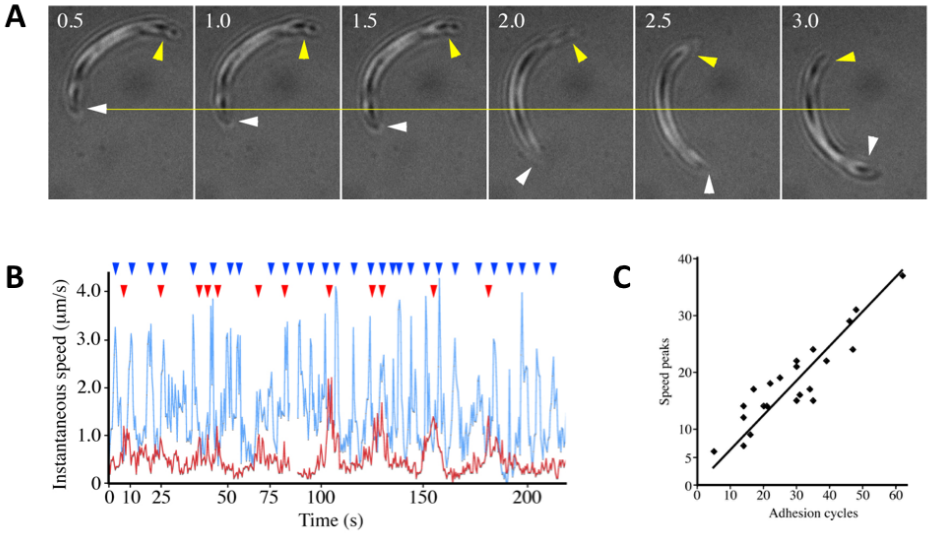

Fig. 3: *(A) A sporozoite that got stuck with the rear end stretches itself until the connection ruptures and motion ensues again. (B) Both a fast (blue) and a slow (red) sporozoite exhibit speed peaks that are characteristic for stick-slip motion. (C) The number of speed peaks correlates with the number of adhesion cycles, demonstrating the close relation between motility and adhesion. Taken from [44].*

iments and it was found that it can be much faster than sporozoite motility, namely 15 μm/s versus 1-2 μm/s [49]. It is driven by an ancient myosin motor, myoA, that interacts with short actin filaments in the narrow space between the inner membrane complex and the plasma membrane, together forming some kind of active fluid , similar to the actin cytoskeleton of animal cells. Because malaria actin does not polymerise into long filaments and also is not known to branch or crosslink, however, this system seems to be quite different from the retrograde flow usually driving migration of animal cells.

While the crescent shape of sporozoites in tissue leads to locally helical trajectories [15], for single sporozoites on planar substrates the combination of crescent shape and retrograde flow along the cell body leads to circular movement [44]. Motion is usually counterclockwise, presumably because chiral symmetry is broken by the microtubule basket anchored at the apical ring. Closer investigation of sporozoite trajectories revealed that circular motion is not homogeneous, but often interrupted by adhesive events. A typical example is shown in Fig. 3A, where the sporozoite gets stuck at the back (yellow arrow). The front continues to move forward (white arrow), thus the cell body stretches and finally the adhesion at the rear is broken and motion ensues again. Fig. 3B shows that many such speed peaks appear during sporozoite motion, irrespective of the average speed of the parasite (here a fast and a slow parasite are shown in blue and red, respectively). Using reflection interference contrast microscopy (RICM) and traction force microscopy (TFM) , it has been shown that small regions of strong adhesion exist between sporozoite and substrate, and that these adhesion sites are highly dynamic. As demonstrated in Fig. 3C, speed peaks correlate with adhesion cycles, demonstrating the close relation between movement and adhesion. Although sporozoites adhere through specific adhesion molecules to their environment, their speed and the stick-slip type motion pattern seem not to depend strongly on the exact nature of the extracellular ligand. In fact such a motion pattern is generic for sliding friction and it has been modelled before also in the context of retrograde

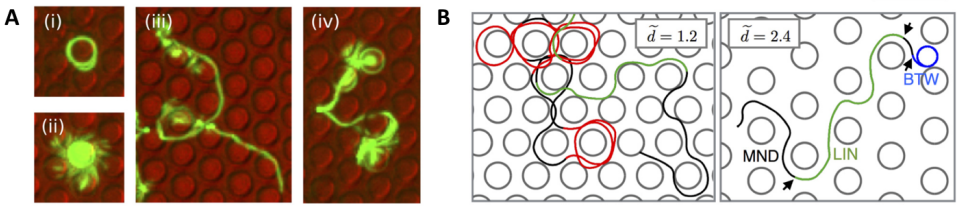

Fig. 4: *(A) Different motility modes are observed for sporozoites in pillar assays: (i) circling, (ii) wavering, (iii) linear and (iv) meandering. (B) An agent-based model for sporozoite motility can be used to predict these different motility modes as a function of lattice constant: circling around pillars (red), circling between pillars (blue), linear (green) and meandering (black). Taken from [15].*

flow of animal cells [50].

Given the circular movement on planar substrates, it is intriguing to ask how the complex motion patterns arise that one can observe for sporozoites *in vivo*. A surprising answer has been provided by the help of pillar assays [16, 17]. PDMS-pillars with similar radii as sporozoites have been microfabricated and used as obstacle arrays for sporozoite migration. As shown in Fig. 4A, many different motion patterns were observed even for the same geometry. This suggests that sporozoite trajectories are mainly determined by the geometry of their extracellular environment. A simple agent-based model for sporozoite motility was therefore used to simulate sporozoite motility in pillar arrays and indeed gave very similar results, compare Fig. 4B [15]. Here the sporozoite was modelled as a self-propelled particle with curvature, bending energy and excluded volume interaction with the pillars. In addition, it was required to allow for complete re-orientation if collisions could not be resolved by bending, in agreement with experimental observations that sporozoites can buckle and loose substrate contact during collisions. Remarkably, it was also found that sporozoites tend to accumulate around pillars with matching radii, suggesting that their curvature has evolved through the interaction with blood capillaries, which have a similar radius.

4 Mechanics and remodelling of infected red blood cells

RBCs are the most abundant cell type in our body. From the estimated $3.1 \cdot 10^{13}$ cells in our body, $2.6 \cdot 10^{13}$ are RBCs [51]. With an average lifetime of 120 days, this implies that we produce 2.6 million new RBCs every second. For a parasitemia of 10%, there will be $2.6 \cdot 10^{12}$ infected RBCs (iRBCs) in the circulation (ca. 200 g of parasitic mass). In principle, this means that in extreme cases, the malaria parasite can outnumber all other cells in our body, including *E. Coli*, of which humans carries approximately equal numbers as own cells (amounting also to 200 g) [52]. Not only are there so many RBCs, each of them is also an ideal host for the parasite, offering nutrients (mainly hemoglobin, which the malaria parasites digest during the 48 h in the iRBC) and protection from the immune system (especially because the parasite is shield by two membranes, the PVM and the RBC-membrane).

Because RBCs do not have a nucleus and are filled with hemoglobin, their mechanics is mainly determined by the cell envelope, a composite of plasma membrane and spectrin cytoskeleton [53]. Moreover their biological function is strongly shaped by physical factors. For these

reasons, they are attractive model systems for biophysical investigations. In particular, there exists a well-developed mathematical and computational framework to understand their shape and mechanics [54] and well as their deformations and movement in shear flow [55]. The mechanics of their plasma membrane is dominated by local bending energy

$$\mathcal{H}_{bend} = 2\kappa \int dA \, (H - c_0)^2 \tag{1}$$

where $dA(u,v) = g(u,v)^{1/2} du dv$ is the integral measure of the surface area, $g(u,v)$ the determinant of the metric tensor, and u and v are the internal coordinates of the surface. $H(u,v)$ is the local mean curvature of the surface, c_0 is the spontaneous curvature and κ is the bending rigidity . In addition one has to take into account the area-difference-elasticity (ADE) arising from a difference in surface areas between the two leaflets

$$\mathcal{H}_{ADE} = \frac{\bar{\kappa}\pi}{2AD^2} \left(\Delta A - \Delta A_0\right)^2 \tag{2}$$

where D is the distance between the two leaflets (typical value 2 nm), $\bar{\kappa}$ the ADE-modulus and the difference in surface area can be calculated as

$$\Delta A = 2D \int dA \, H \; . \tag{3}$$

This shows that spontaneous curvature c_0 and area difference ΔA_0 have a similar effect and cannot be extracted independently of each other.
The mechanics of the spectrin-actin cytoskeleton underlying the plasma membrane is described by thin shell elasticity

$$\mathcal{H}_{elast} = \int dA \left(\frac{K_\alpha}{2} \alpha^2 + \mu\beta \right) \tag{4}$$

with the 2D stretch modulus K_α and the 2D shear modulus μ . Area and shear strain, respectively, follow from the principal extension ratios λ_1 and λ_2 of a deformed ellipse as

$$\alpha = \lambda_1\lambda_2 - 1, \; \beta = \frac{1}{2}\left(\frac{\lambda_1}{\lambda_2} + \frac{\lambda_2}{\lambda_1} - 2 \right) \; . \tag{5}$$

To evalute the elastic energy, one has to define a reference shape. Additionally one can consider higher order terms, which become important at large deformations, where typically strain stiffening occurs due to the polymeric nature of the spectrin network. Finally bending and thin shell elasticity energies have to be complemented by Lagrange parameters to enforce constant area and volume.
Wildtype RBCs have a typical surface area of $A = 140 \; \mu m^2$ and a typical volume of $V = 100 \; \mu m^3 = 100$ fl [57, 56]. The surface area of a sphere with the same volume would be $A = 104 \; \mu m^2$, thus the RBC has an excess area over the equivalent sphere of around 40%. Another way to express this important relation is to define the reduced volume

$$v = \frac{V}{V_0} = \frac{6\sqrt{\pi}V}{A^{3/2}} \tag{6}$$

which is the real volume V in relation to the volume of a sphere with the same area A. The RBC has $v = 0.64$, again indicating the high degree of excess area. The classical values for the elastic parameters are $\kappa \approx 50 \; k_B T$, $K_\alpha \approx 25 \; \kappa/\mu m^2$ and $\mu \approx K_\alpha/2 = 2.5 \; \mu N/m$ [58].

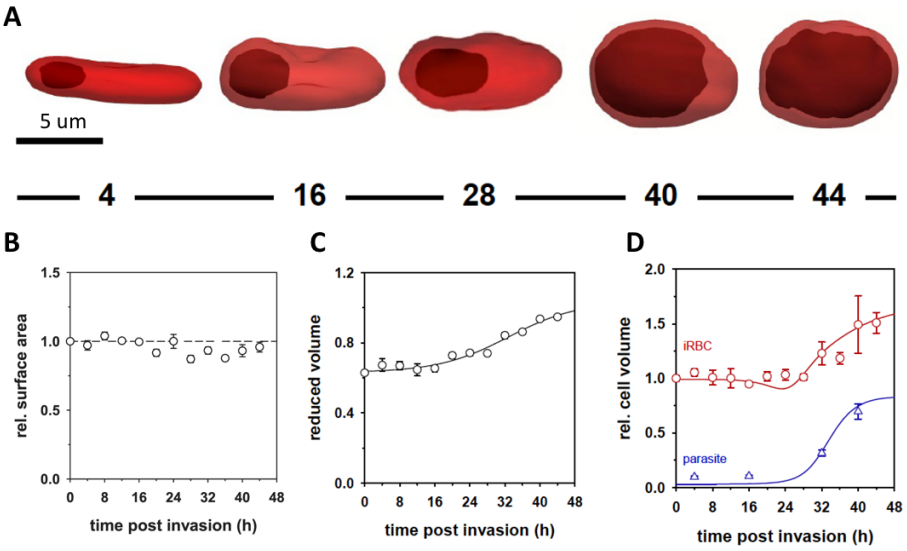

Fig. 5: *(A) Shape of iRBC and parasite mass inside over the complete time of the 48 h asexual cycle as extracted by image processing from confocal stacks. One clearly sees that the parasite rounds up and moves towards the center of the iRBC, and that the iRBC itself also becomes round. (B-D) Time course of surface area and volume of iRBCs extracted from the image processed data. While surface area stays roughly constant, volume goes up by* 60%*. Solid lines are the predictions of the colloid-osmotic model. Adapted from [56].*

Impressively, this theoretical framework gives rise to a complete understanding of the large zoo of RBC-shapes, including the stomatocyte-discocyte-echinocyte sequence arising from changing differential area [58] and the echinocytic shapes that arise as bilayer budding effected by large spontaneous curvature or differential area, but suppressed by elasticity [59]. For the wild-type RBC with the values reported above , the discocyte arises as the stable solution mainly due to the bending energy at reduced volume $v = 0.64$. The interface Hamiltonian for RBCs also suggests that the echinocytosis observed after merozoite invasion is related to some change in membrane composition, which has this global effect on RBC-shape.

It is a long-standing question how RBC standard shape is changed during the course of a malaria-infection. As shown in Fig. 5, the time course of the shape of iRBCs (A) and from this also the time courses of area (B) and volume (C,D) as a function of developmental time recently have been measured with high resolution [56]. In general, these measurements confirm earlier results that the iRBC starts to round up at around 20 h post invasions, at the same time when the parasite mass starts to grow and to move into the center. In regard to area and volume, it was found that surface area A is relatively constant, but that volume V increased by 60% (that is to $V = 160\ \mu m^3$) from late ring to schizont, in very good agreement with the predictions of the colloid-osmotic model [26], but in contrast to earlier work that reported a reduction of A at relatively constant V [60, 61]. In particular, these data imply that the schizont has a reduced volume v close to 1 and thus can be modeled as a round cell in regard to its movement in hydrodynamic flow.

Another central issue are the values of the elastic parameters defined by the composite interface Hamiltonian introduced above. By fitting a multiscale model similar to the above continuum model to experimental deformation data from optical tweezer experiments, it was found that the

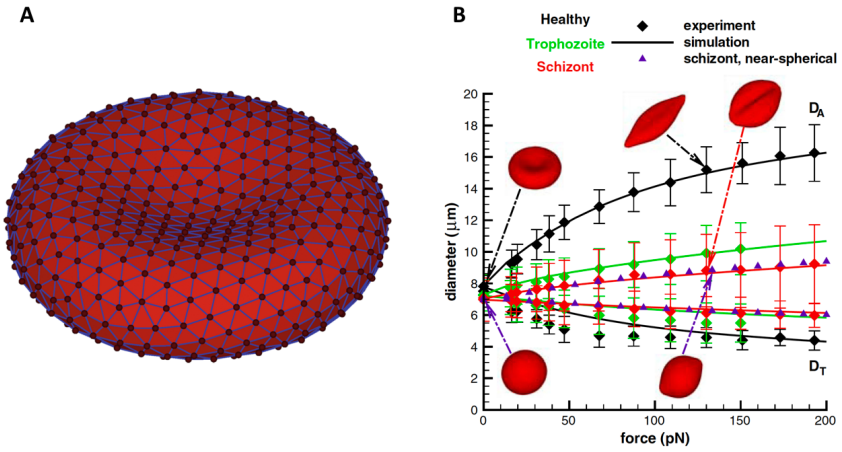

Fig. 6: *(A) Representation of a biconcave wildtype RBC as a triangulated surface in a multiscale model that incorporates both bending and elastic energies. Taken from [55]. (B) Experimental and simulated force-deformation curves for stretched RBCs. One clearly sees that iRBCs become much stiffer as they develop from wildtype through trophozoite to schizont. Taken from [62].*

wildtype 2D shear modulus should be $\mu = 8.3\ \mu N/m$ and that the bending modulus κ should be larger than $50\ k_BT$ [63]. A similar result, $\mu = 4.73\ \mu N/m$ and κ in the range of $100\ k_BT$, was found by a multiscale model that also incorporates dynamical effects [64]. Fitting stretching data for iRBCs, it was found that the shear modulus μ increases to $14.5\ \mu N/m$, $29\ \mu N/m$ and $40\ \mu N/m$ for ring, trophozoite and schizont stages [62], compare Fig. 6. This dramatic increase in stiffness underscores the fact that the parasite is under large evolutionary pressure to avoid passage through the spleen, where stiff RBCs are sorted out. Based on the AFM imaging data of the changes in the spectrin network over the 48 h asexual cycle [33], a multiscale model has been parametrized that suggests that the stiffness increase results mainly from the vertical links between the knobs and the spectrin network [34].
For the movement of RBCs in shear flow, we also have to know its viscoelastic properties. Their mean hemoglobin concentration is 33 g/dl and leads to an intracellular viscosity of $6 \cdot 10^{-3}$ Pa s, five times higher than the viscosity of the surrounding blood plasma. Higher hemoglobin concentrations would lead to a strong increase in viscosity. Due to ageing, RBCs loose surface area and volume, but not hemoglobin, leading to a strong reduction in cell deformability and removal in the spleen. These observations might explain why the malaria parasite seems to digest more hemoglobin than needed for its own metabolism.

5 Cytoadhesion of infected red blood cells

Malaria parasites induce cytoadherence of iRBCs in order to increase residency time in the vasculature and to avoid clearance by the spleen. To this end, they export proteins like KAHRP and PfEMP1 that self-assembly into thousands of adhesive knobs on the surface of the iRBC. While the diameter of these knobs becomes smaller during the asexual cycle, its height stays constant at a value of 10-20 nm, as measured with SEM and AFM [65, 66, 67]. Strikingly,

this design is similar to the one evolved by leukocytes, which use rolling adhesion to scan the endothelium for signals of inflammation [68]. To this end, they localize adhesion molecules from the selectin family to the tips of hundreds of microvilli covering their surfaces. Therefore it has been suggested that this common design of multiple adhesive protrusions is the result of an optimalisation process for cell capture and adhesion under flow conditions [69, 70, 71]. Another striking observation is the observation that iRBC-adhesion is flow-enhanced [72], as also known from leukocytes [73] and bacteria [74]. Often such behaviour results from molecular catch bonds (whose lifetime increases with force, in contrast to a decrease for the usual slip bonds) and indeed a very recent study has reported that the PfEMP1:ICAM1 bond has this property [75].

To model cytoadhesion of iRBCs in shear flow, one first needs to choose a suitable method to describe movement of the cell in hydrodynamic flow . For spherical cells, such a method has been introduced by Hammer and coworkers, who simulated the phase diagram of rolling adhesions for leukocytes [76, 77]. In later studies, this method has been extended to also resolve the receptors on the cell surface and the ligands on the substrates [70, 78, 79]. Recently this approach has also been applied to cytoadhesion of schizonts [80], because these can be considered to be round cells, compare Fig. 5. In essence, adhesive dynamics for round cells is the simulation of a Langevin equation

$$\partial_t X(t) = u^\infty + M\{F_S + F_D\} + k_B T \nabla M + \xi(t), \tag{7}$$

where $X(t)$ is a six-dimensional vector describing translation and rotation of the spherical cell. M is a mobility matrix that can be calculated semi-analytically from the solution of the Stokes equation for a sphere above a wall. u^∞ is the imposed linear shear flow and F_S and F_D are shear and direct forces, respectively, with the former also resulting from the Stokes equation and the latter including the adhesion forces. $\xi(t)$ is the usual random force/torque and the term with ∇M arises due to the multiplicative noise. Additional model parameters are the rules for bond association and dissociation. Usually one assumes a constant on-rate below a typical encounter distance and an off-rate that depends exponentially on force according to the Bell-Evans-model for slip bonds. Finally one has to define the exact distribution of receptors and ligands. As shown in Fig. 7A, for schizonts one can model the clustering of PfEMP1-molecules into knobs, while the corresponding ligands are distributed with a typical distance on the substrate. In Fig. 7B it is shown that with this model, one can achieve good agreement with flow chamber experiments for rolling velocity as a function of shear rate. In particular, this work predicts that a typical number of PfEMP1-molecules per knob (*multiplicity*) should be six, in agreement with earlier estimates [81].

In order to also describe the other stages of the asexual cycle, when the iRBCs are not spherical, one has to implement a hydrodynamic method that can also deal with deformable cells. The same challenge in fact arises also for wildtype RBCs. One approach often applied to simulate blood flow is the Lattice Boltzmann Method (LBM) [82]. More recently, however, the movement of RBCs in shear flow has been simulated also with other methods, in particular with Multiparticle Collision Dynamics (MPCD) [83] and Dissipative Particle Dynamics (DPD) [84, 64]. These hydrodynamic methods are then coupled to the elasticity of the RBC, compare Fig. 6A, often implementing a multiscale model that in the continuum limit becomes the interface Hamiltonian described above. These approaches can predict many effects observed in blood flow, in particular the parachute shape of single RBCs in channel flow, the Fahraeus-Lindqvist effect (decrease of apparent viscosity with decreasing channel diameter) and the margination of white blood cells [55]. Cytoadhesion of trophozoites has been simulated with the DPD-approach and

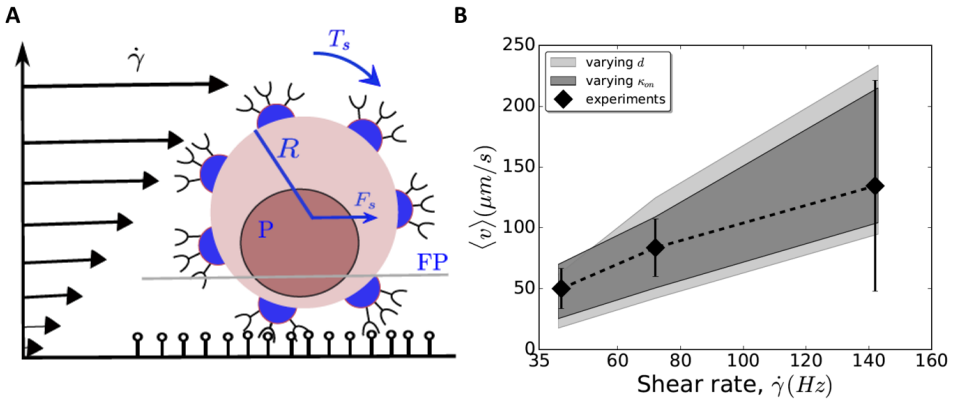

Fig. 7: *(A) Model for a round cell adhering in linear shear flow through adhesive knobs on its surface. Shear flow generates both a translational force F_s and a torque T_s. A fluorescent parasite mass (P) can be used to characterize rotation because it will oscillate as it goes in and out of the focal plane (FP). (B) Comparison of experimental and simulation data for rolling velocity as a function of shear rate with reasonable corridors for the model parameters (light shaded: 100 to 400 nm in ligand distance; dark shaded: 0.1 to 10 Hz in on-rate). Taken from [80].*

revealed that these should flip rather than roll in shear flow due to their biconcave shape and smaller stiffness [62, 85], as recently indeed confirmed by flow chamber experiments [80].

6 Conclusions and outlook

As it is true for all pathogens, the malaria parasite is both frightening and fascinating to any researcher who studies the ways in which it interacts with its hosts. One of the most surprising aspects of the lifecycle is the observation how strongly the organization of the parasite depends on the environment with which it interacts. For example, when one compares the architecture of the sporozoite from Fig. 2A with the one of the merozoite from Fig. 2B, one cannot help to be surprised by the much larger size (10 versus 1 μm) and completely different shape (crescent versus egg) of the two variants, which both arise from the same genome. Obviously these different architectures correspond to very different functions, namely fast motility in the skin versus invasion of RBCs in the blood. Evolutionary adaptability also becomes apparent in many other cellular functions described here. In particular, we have seen that the motion patterns of sporozoites are strongly shaped by their environment, as revealed by the pillar assays, and that the cytoadhesion of iRBCs mimics the way leukocytes interact adhesively with the endothelium, as confirmed by the adhesive dynamics simulations.

Although the malaria parasite is very special due to its unique lifecycle, the main biophysical questions that arise during its investigation are very similar to the ones that one also studies for other cell types. Here we have focused on two main stages in the human host, namely the skin and blood stages. For the sporozoite, which seems to be optimised for fast motion through the skin in search for blood vessels, we have seen that fast motility is achieved by retrograde flow of surface-anchored adhesins, and that simple physics models for sliding friction and self-propelled particles can explain some of its peculiar motion features. One open question in this context is the question how retrograde flow is accomplished by the interplay between the

myosin motor and actin, which in contrast to the lamellipodium of migrating animal cells does not seem to form long and branched or crosslinked filaments. Another open question in the sporozoite field is the question why the parasite has evolved very specific adhesion molecules when *in vitro* it does not need any special ligands to achieve its high level of motility.
Merozoites seem to be optimised for efficient invasion of RBCs and lead to a complete remodelling of the iRBC. Because RBCs are an extremely well-studied subject in biophysics, including mature theories for their shape, mechanics and movement in hydrodynamic flow, the biophysics of iRBCs has developed as a very fruitful sub-area of this large field. One additional aspect not present in healthy RBCs is cytoadherence of iRBCs, which has led to the development of adhesive dynamics simulations of both round and deformable cells. At the current stage, one of the main challenges is to establish a tighter connection to the underlying molecular processes through multiscale approaches. For example, it is still unclear how exactly the parasite remodels the spectrin network, how it controls transport through the cytoplasm and the different membranes, which variants of the adhesion molecule PfEMP1 are expressed in which context, how the endothelium reacts to different variants of iRBCs, and if and how iRBCs interact with other cells in the blood flow.
Finally we note that the liver stage, the sexual blood stage and the mosquito stages as described above are still largely *terra incognita* from the viewpoint of biophysics. Without doubt, the parasite has evolved unexpected solutions also for these stages. As is the case with all pathogens, one can only hope that understanding these mechanisms in more details also will provide better ways to fight this deadly disease.

Acknowledgments: I would like to thank all past and present members of the Heidelberg community working on the biophysics of malaria for helpful discussions and enjoyable collaborations, in particular Friedrich Frischknecht, Joachim Spatz, Sylvia Münter, Benedikt Sabass, Christine Selhuber, Anna Battista, Michael Lanzer, Anil Kumar Dasanna, Motomu Tanaka and Julia Jäger. This work was supported by the DFG Collaborative Research Center 1129 on Integrative analysis of pathogen replication and spread at Heidelberg.

References

[1] L. H. Miller, D. I. Baruch, K. Marsh, and O. K. Doumbo, Nature **415**(6872), 673 (2002).

[2] World health organization (WHO), *World malaria report 2016*.

[3] B. M. Cooke, N. Mohandas, and R. L. Coppel, Seminars in Hematology **41**(2), 173 (2004).

[4] M. Cyrklaff, C. P. Sanchez, F. Frischknecht, and M. Lanzer, Trends in Parasitology **28**(11), 479 (2012).

[5] S. Suresh, J. Spatz, J. P. Mills, A. Micoulet, M. Dao, C. T. Lim, M. Beil, and T. Seufferlein, Acta Biomaterialia **1**, 15 (2005).

[6] G. Y. H. Lee and C. T. Lim, Trends in Biotechnology **25**(3), 111 (2007).

[7] D. A. Fedosov, Drug Discovery Today: Disease Models **16**, 17 (2015).

[8] U. S. Schwarz, Seminars in Cell & Developmental Biology **46**(Supplement C), 82 (2015).

[9] R. E. Mebius and G. Kraal, Nature Reviews Immunology **5**(8), 606 (2005).

[10] I. V. Pivkin, Z. Peng, G. E. Karniadakis, P. A. Buffet, M. Dao, and S. Suresh, Proceedings of the National Academy of Sciences **113**(28), 7804 (2016).

[11] J. Baum and F. Frischknecht, Seminars in Cell & Developmental Biology **46**(Supplement C), 78 (2015).

[12] A. Hochstetter and T. Pfohl, Trends in Parasitology **0**(0) (2016).

[13] M. De Niz, P.-C. Burda, G. Kaiser, H. A. del Portillo, T. Spielmann, F. Frischknecht, and V. T. Heussler, Nature Reviews Microbiology **15**(1), 37 (2017).

[14] R. Amino, S. Thiberge, B. Martin, S. Celli, S. Shorte, F. Frischknecht, and R. Mnard, Nature Medicine **12**(2), 220 (2006).

[15] A. Battista, F. Frischknecht, and U. S. Schwarz, Physical Review E **90**(4), 042720 (2014).

[16] J. K. Hellmann, S. Mnter, M. Kudryashev, S. Schulz, K. Heiss, A.-K. Mller, K. Matuschewski, J. P. Spatz, U. S. Schwarz, and F. Frischknecht, PLoS Pathog **7**(6), e1002080 (2011).

[17] M. J. Muthinja, J. Ripp, J. K. Hellmann, T. Haraszti, N. Dahan, L. Lemgruber, A. Battista, L. Schtz, O. T. Fackler, U. S. Schwarz, J. P. Spatz, and F. Frischknecht, Advanced Healthcare Materials pp. n/a–n/a (2017).

[18] K. Keren, Z. Pincus, G. M. Allen, E. L. Barnhart, G. Marriott, A. Mogilner, and J. A. Theriot, Nature **453**(7194), 475 (2008).

[19] M. Dembo and Y.-L. Wang, Biophysical Journal **76**(4), 2307 (1999).

[20] A. F. Cowman and B. S. Crabb, Cell **124**(4), 755 (2006).

[21] A. F. Cowman, D. Berry, and J. Baum, J Cell Biol **198**(6), 961 (2012).

[22] I. Tardieux and J. Baum, The Journal of Cell Biology **214**(5), 507 (2016).

[23] P. R. Gilson and B. S. Crabb, International Journal for Parasitology **39**(1), 91 (2009).

[24] S. Dasgupta, T. Auth, N. Gov, T. Satchwell, E. Hanssen, E. Zuccala, D. Riglar, A. Toye, T. Betz, J. Baum, and G. Gompper, Biophysical Journal **107**(1), 43 (2014).

[25] A. Crick, M. Theron, T. Tiffert, V. Lew, P. Cicuta, and J. Rayner, Biophysical Journal **107**(4), 846 (2014).

[26] J. M. A. Mauritz, A. Esposito, H. Ginsburg, C. F. Kaminski, T. Tiffert, and V. L. Lew, PLoS Comput Biol **5**(4), e1000339 (2009).

[27] L. G. Pologe, A. Pavlovec, H. Shio, and J. V. Ravetch, Proceedings of the National Academy of Sciences **84**(20), 7139 (1987).

[28] B. S. Crabb, B. M. Cooke, J. C. Reeder, R. F. Waller, S. R. Caruana, K. M. Davern, M. E. Wickham, G. V. Brown, R. L. Coppel, and A. F. Cowman, Cell **89**(2), 287 (1997).

[29] H. Weng, X. Guo, J. Papoin, J. Wang, R. Coppel, N. Mohandas, and X. An, Biochimica et Biophysica Acta (BBA) - Biomembranes **1838**(1, Part B), 185 (2014).

[30] J. M. Watermeyer, V. L. Hale, F. Hackett, D. K. Clare, E. E. Cutts, I. Vakonakis, R. A. Fleck, M. J. Blackman, and H. R. Saibil, Blood pp. blood–2015–10–674002 (2015).

[31] D. I. Baruch, B. L. Pasloske, H. B. Singh, X. Bi, X. C. Ma, M. Feldman, T. F. Taraschi, and R. J. Howard, Cell **82**(1), 77 (1995).

[32] R. M. Fairhurst, D. I. Baruch, N. J. Brittain, G. R. Ostera, J. S. Wallach, H. L. Hoang, K. Hayton, A. Guindo, M. O. Makobongo, O. M. Schwartz, A. Tounkara, O. K. Doumbo, *et al.*, Nature **435**(7045), 1117 (2005).

[33] H. Shi, Z. Liu, A. Li, J. Yin, A. G. L. Chong, K. S. W. Tan, Y. Zhang, and C. T. Lim, PLOS ONE **8**(4), e61170 (2013).

[34] Y. Zhang, C. Huang, S. Kim, M. Golkaram, M. W. A. Dixon, L. Tilley, J. Li, S. Zhang, and S. Suresh, Proceedings of the National Academy of Sciences **112**(19), 6068 (2015).

[35] M. Cyrklaff, C. P. Sanchez, N. Kilian, C. Bisseye, J. Simpore, F. Frischknecht, and M. Lanzer, Science **334**(6060), 1283 (2011).

[36] R. M. Fairhurst, C. D. Bess, and M. A. Krause, Microbes and Infection **14**(10), 851 (2012).

[37] L. Bannister, J. Hopkins, R. Fowler, S. Krishna, and G. Mitchell, Parasitology Today **16**(10), 427 (2000).

[38] M. Abkarian, G. Massiera, L. Berry, M. Roques, and C. Braun-Breton, Blood **117**(15), 4118 (2011).

[39] A. Callan-Jones, O. AlbarranArriagada, G. Massiera, V. Lorman, and M. Abkarian, Biophysical Journal **103**(12), 2475 (2012).

[40] M. Aingaran, R. Zhang, S. K. Law, Z. Peng, A. Undisz, E. Meyer, M. Diez-Silva, T. A. Burke, T. Spielmann, C. T. Lim, S. Suresh, M. Dao, *et al.*, Cellular Microbiology **14**(7), 983 (2012).

[41] M. Dearnley, T. Chu, Y. Zhang, O. Looker, C. Huang, N. Klonis, J. Yeoman, S. Kenny, M. Arora, J. M. Osborne, R. Chandramohanadas, S. Zhang, *et al.*, Proceedings of the National Academy of Sciences **113**(17), 4800 (2016).

[42] D. Klug and F. Frischknecht, eLife **6**, e19157 (2017).

[43] L. D. Sibley, Science **304**(5668), 248 (2004).

[44] S. Muenter, B. Sabass, C. Selhuber-Unkel, M. Kudryashev, S. Hegge, U. Engel, J. P. Spatz, K. Matuschewski, U. S. Schwarz, and F. Frischknecht, Cell Host & Microbe **6**(6), 551 (2009).

[45] M. B. Heintzelman, Seminars in Cell & Developmental Biology **46**(Supplement C), 135 (2015).

[46] T. Mignot, J. W. Shaevitz, P. L. Hartzell, and D. R. Zusman, Science **315**(5813), 853 (2007).

[47] R. Balagam, D. B. Litwin, F. Czerwinski, M. Sun, H. B. Kaplan, J. W. Shaevitz, and O. A. Igoshin, PLOS Computational Biology **10**(5), e1003619 (2014).

[48] S. T. Islam and T. Mignot, Seminars in Cell & Developmental Biology **46**(Supplement C), 143 (2015).

[49] K. A. Quadt, M. Streichfuss, C. A. Moreau, J. P. Spatz, and F. Frischknecht, ACS Nano **10**(2), 2091 (2016).

[50] B. Sabass and U. S. Schwarz, Journal of Physics: Condensed Matter **22**, 194112 (2010).

[51] R. Milo and R. Phillips, *Cell Biology by the Numbers* (Garland Science, 2015), google-Books-ID: 9NPRCgAAQBAJ.

[52] R. Sender, S. Fuchs, and R. Milo, PLOS Biology **14**(8), e1002533 (2016).

[53] S. E. Lux, Blood **127**, 187 (2015).

[54] Lim, H.W.G., Wortis, M., and Mukhopadhyay. R., in *Soft Matter* (Wiley-VCH Verlag GmbH & Co. KGaA, 2008), vol. 4, pp. 83–249.

[55] D. A. Fedosov, H. Noguchi, and G. Gompper, Biomechanics and Modeling in Mechanobiology **13**(2), 239 (2014).

[56] M. Waldecker, A. K. Dasanna, C. Lansche, M. Linke, S. Srismith, M. Cyrklaff, C. P. Sanchez, U. S. Schwarz, and M. Lanzer, Cellular Microbiology **19**(2), 1 (2017).

[57] N. Mohandas and P. G. Gallagher, Blood **112**(10), 3939 (2008).

[58] G. L. H. W, M. Wortis, and R. Mukhopadhyay, Proceedings of the National Academy of Sciences **99**(26), 16766 (2002).

[59] R. Mukhopadhyay, H. W. Gerald Lim, and M. Wortis, Biophysical Journal **82**(4), 1756 (2002).

[60] A. Esposito, J.-B. Choimet, J. N. Skepper, J. M. A. Mauritz, V. L. Lew, C. F. Kaminski, and T. Tiffert, Biophysical Journal **99**(3), 953 (2010).

[61] I. Safeukui, P. A. Buffet, S. Perrot, A. Sauvanet, B. Aussilhou, S. Dokmak, A. Couvelard, D. C. Hatem, N. Mohandas, P. H. David, O. Mercereau-Puijalon, and G. Milon, PLOS ONE **8**(3), e60150 (2013).

[62] D. A. Fedosov, B. Caswell, S. Suresh, and G. E. Karniadakis, Proceedings of the National Academy of Sciences **108**(1), 35 (2011).

[63] J. Li, M. Dao, C. T. Lim, and S. Suresh, Biophysical Journal **88**(5), 3707 (2005).

[64] D. A. Fedosov, B. Caswell, and G. E. Karniadakis, Biophysical Journal **98**(10), 2215 (2010).

[65] J. Gruenberg, D. R. Allred, and I. W. Sherman, The Journal of Cell Biology **97**(3), 795 (1983).

[66] E. Nagao, O. Kaneko, and J. A. Dvorak, Journal of Structural Biology **130**(1), 34 (2000).

[67] K. A. Quadt, L. Barfod, D. Andersen, J. Bruun, B. Gyan, T. Hassenkam, M. F. Ofori, and L. Hviid, PLoS ONE **7**(9), e45658 (2012).

[68] T. Springer, Cell **76**(2), 301 (1994).

[69] M. Ho, M. J. Hickey, A. G. Murray, G. Andonegui, and P. Kubes, The Journal of Experimental Medicine **192**(8), 1205 (2000).

[70] C. Korn and U. S. Schwarz, Physical Review Letters **97**(13), 138103 (2006).

[71] G. Helms, A. K. Dasanna, U. S. Schwarz, and M. Lanzer, FEBS Letters **590**(13), 1955 (2016).

[72] H. Rieger, H. Y. Yoshikawa, K. Quadt, M. A. Nielsen, C. P. Sanchez, A. Salanti, M. Tanaka, and M. Lanzer, Blood **125**(2), 383 (2015).

[73] R. Alon, D. A. Hammer, and T. A. Springer, , Published online: 06 April 1995; | doi:10.1038/374539a0 **374**(6522), 539 (1995).

[74] W. E. Thomas, E. Trintchina, M. Forero, V. Vogel, and E. V. Sokurenko, Cell **109**(7), 913 (2002).

[75] Y. B. Lim, J. Thingna, J. Cao, and C. T. Lim, Scientific Reports **7**(1), 4208 (2017).

[76] D. A. Hammer and S. M. Apte, Biophysical Journal **63**(1), 35 (1992).

[77] K.-C. Chang, D. F. J. Tees, and D. A. Hammer, Proceedings of the National Academy of Sciences **97**(21), 11262 (2000).

[78] C. B. Korn and U. S. Schwarz, The Journal of Chemical Physics **126**(9), 095103 (2007).

[79] C. B. Korn and U. S. Schwarz, Physical Review E **77**(4), 041904 (2008).

[80] A. K. Dasanna, C. Lansche, M. Lanzer, and U. S. Schwarz, Biophysical Journal **112**(9), 1908 (2017).

[81] X. Xu, A. K. Efremov, A. Li, L. Lai, M. Dao, C. T. Lim, and J. Cao, PLoS ONE **8**(5), e64763 (2013).

[82] C. Sun, C. Migliorini, and L. L. Munn, Biophysical Journal **85**(1), 208 (2003).

[83] H. Noguchi and G. Gompper, Proceedings of the National Academy of Sciences of the United States of America **102**(40), 14159 (2005).

[84] I. V. Pivkin and G. E. Karniadakis, Physical Review Letters **101**(11), 118105 (2008).

[85] D. Fedosov, B. Caswell, and G. Karniadakis, Biophysical Journal **100**(9), 2084 (2011).